

Oriented Monolayers Prepared from Lyotropic Chromonic Liquid Crystal

Tod Schneider,[†] Kateryna Artyushkova,[‡] Julia E. Fulghum,[‡] Laurie Broadwater,[§] Ashley Smith,^{†,||} and Oleg D. Lavrentovich^{*,†}

Chemical Physics Interdisciplinary Program and Liquid Crystal Institute, and Chemistry Department, Kent State University, Kent, Ohio 44242, and Chemical and Nuclear Engineering Department, University of New Mexico, Albuquerque, New Mexico 87131

Received September 3, 2004. In Final Form: January 10, 2005

We use a layer-by-layer electrostatic self-assembly technique to obtain in-plane oriented aggregates of mesogenic dye molecules cast from lyotropic chromonic liquid crystals (LCLCs) on mica substrates. The aqueous solutions of dye used for deposition are in the nematic phase. Atomic force microscopy and X-ray photoelectron spectroscopy of the dried film reveal that the LCLC molecules adsorb at the charged substrate preserving ordered aggregates of elongated shape characteristic of the nematic phase in the aqueous solution. These elongated aggregates of LCLC molecules form films with in-plane orientational order and are compositionally distinct from the substrate.

Introduction

Organic films with nanoscale order produced by self-assembly at solid substrates have generated much interest in recent years.^{1,2} Modern technologies of molecular self-assembly use the noncovalent association of molecules into aggregates of nanometer size.³ One of the proven strategies, the technique of adsorption of charged colloidal particles through electrostatic interactions on a layer-by-layer basis, was developed by Iler⁴ in 1965 following the early work of Langmuir.⁵ Recently, we described the production of mono- and multimolecular films with long-range in-plane orientational order.⁶ These films were created layer-by-layer through electrostatic deposition from the so-called lyotropic chromonic liquid crystal (LCLC)^{7,8} formed by aqueous solutions of certain mesogenic dyes. The molecular structure and mesogenic macrostructure of LCLCs are manifestly different from those of conventional surfactant-type lyotropic liquid crystals. The LCLC molecules are usually planklike rather than rodlike, rigid rather than flexible, and aromatic rather than aliphatic. In addition, LCLC molecules aggregate into columns as opposed to forming the closed micelles typical of surfactant amphiphiles.⁹ LCLCs generally contain hydrophilic ionic groups at the periphery of

the molecule that solubilize the material in water. These ionic groups at the extremities of the molecule can be employed in a scheme of electrostatic adsorption onto an oppositely charged surface, such as a substrate coated with polyelectrolytes.⁶ In such a scheme, the charged surfaces of the LCLC columns form electrostatic bonds with the charged substrate, thereby fixing the orientation of the column as it is adsorbed in the plane of the substrate. If the material is shear-deposited from the N phase, the columns will generally align along the direction of (shear) deposition. (Other directions are also possible, depending on the viscoelastic properties of the LCLC material and the anisotropic nature of the substrate; see Results.) Excess material can be washed off so that only a monolayer remains and the long-range orientational order within the dye layer is retained. The long-range orientational order can be confirmed by measuring absorption of linearly polarized light as a function of the angle between the polarization direction and the orientation of the LCLC aggregates.⁶ It is significant that deposition from the isotropic phase (higher dilution of the LCLC material in water at the time of deposition) generally produces no in-plane orientational order.⁶

Interestingly, freezing the structure of an LCLC in place to form an oriented film was actually first claimed in the patents of Dreyer in the mid-to-late 1940s and early 1950s.^{10–13} Dreyer first disclosed methods to create oriented films for optical polarizers in 1946: "...I apply polarizable materials in solution or in a fused condition into juxtaposition to an oriented surface, or otherwise into an orienting field, and then, by bringing the polarizable material into the nematic (N) state, I produce a noncrystalline polarizing material oriented in conformity to the orientation of said surface or other orienting field; and thereafter I fix the orientation in such material by controlled solidification." Dreyer was creating oriented thin films of LCLC (probably on the order of hundreds of nanometers thick) 30 years before there was even a

* Address correspondence to this author. Telephone: (330) 672-4844. E-mail: odl@lci.kent.edu.

[†] Chemical Physics Interdisciplinary Program and Liquid Crystal Institute, Kent State University.

[‡] University of New Mexico.

[§] Chemistry Department, Kent State University.

^{||} Work was performed during the Kent State University Undergraduate Summer Research Program 2000.

(1) Tredgold, R. H. *Order in Thin Organic Films*; Cambridge University Press: Cambridge, 1994; p 200.

(2) Decher, G. *Molecular Multilayer Films*. In *Photonic and Optoelectronic Polymers*; American Chemical Society: Washington, DC, 1997; pp 445–459.

(3) Whitesides, G. M.; Mathias, J. P.; Seto, C. T. *Science* **1991**, *254*, 1312.

(4) Iler, R. K. *J. Colloid Interface Sci.* **1966**, *21*, 569.

(5) Langmuir, I. U.S. Patent 2,232,539, 1941.

(6) Schneider, T.; Lavrentovich, O. D. *Langmuir* **2000**, *16*, 5227–5230.

(7) Lydon, J. *Chromonics*. In *Handbook of Liquid Crystals*; Wiley-VCH: Weinheim, 1998; Vol. 2B, p 981. Lydon, J. *Curr. Opin. Colloid Interface Sci.* **1998**, *3*, 458.

(8) Lydon, J. *Curr. Opin. Colloid Interface Sci.* **2004**, *8*, 480.

(9) Kleman, M.; Lavrentovich, O. D., *Soft Matter Physics: An Introduction*; Springer: New York, 2003; p 638.

(10) Dreyer, J. F. U.S. Patent 2,400,877, 1946.

(11) Dreyer, J. F. U.S. Patent 2,481,830, 1949.

(12) Dreyer, J. F. U.S. Patent 2,524,286, 1950.

(13) Dreyer, J. F. U.S. Patent 2,544,659, 1951.

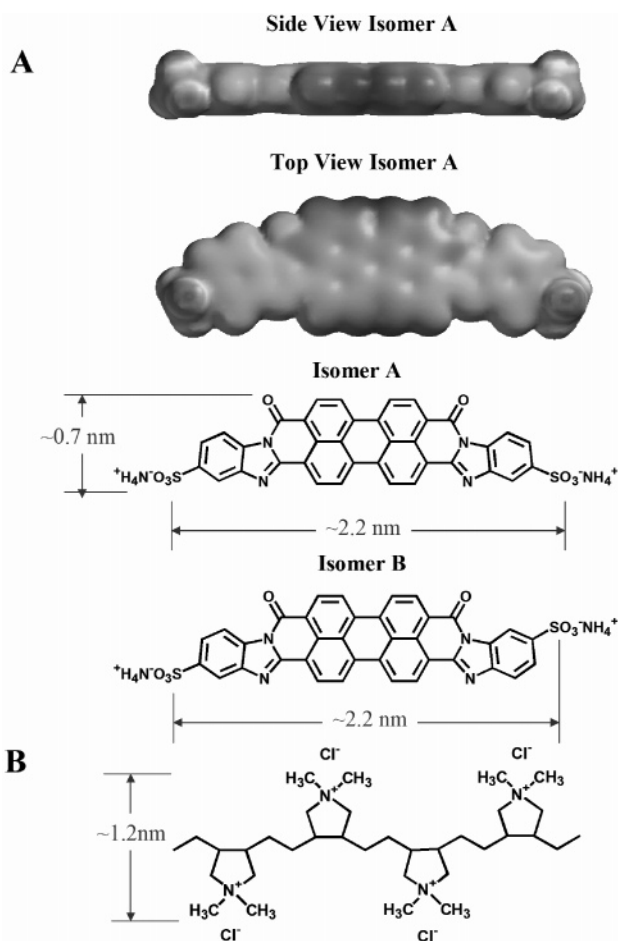


Figure 1. (A) Isomers of Violet 20 [V20] and molecular models showing equilibrium geometry and charge distribution. In aqueous solutions, the ammonium cation dissociates, leaving the molecule negatively charged. Note the flat polyaromatic core. (B) Poly(diallyldimethylammonium chloride) [PDDA], a polyanion used as a binder to stick V20 to the substrate.

rudimentary description of the class of materials he was dealing with. In this work, we wish to extend Dreyer's pioneering work on LCLCs by imaging and determining the structure of orientationally ordered thin films as they are cast from the nematic LCLC aqueous solutions onto solid substrates. We describe atomic force microscopy (AFM) studies¹⁴ of aggregates formed by LCLCs at mica substrates as well as compositional surface analysis by X-ray photoelectron spectroscopy (XPS). Both techniques confirm the long-range orientational order in the plane of the dried films.

Experimental Section

The dye used in this experiment, Violet 20 (V20, $C_{36}H_{22}N_6O_8S_2$, Figure 1A) is available from Optiva, Inc.¹⁵ It has a typical chromogenic structure: a rigid planar polyaromatic core with ammonium counterions at the periphery.⁷ The ammonium groups dissociate in aqueous solutions, leaving the molecule negatively charged by the remaining sulfate groups. In bulk solutions, the planar cores of the molecules attract each other, thus avoiding contact with water. The resulting aggregates are believed to be of columnar type as the planes of the molecules form stacks (rather than closed micelles common in amphiphilic systems).⁷ At sufficiently high concentrations, the columns form liquid crystalline mesophases: the long axes of columns are on average aligned

(14) AFM images presented at MRS Fall Symposium 2000 Boston, MA.

(15) Detailed information can be found at the URL <http://www.optivainc.com/>.

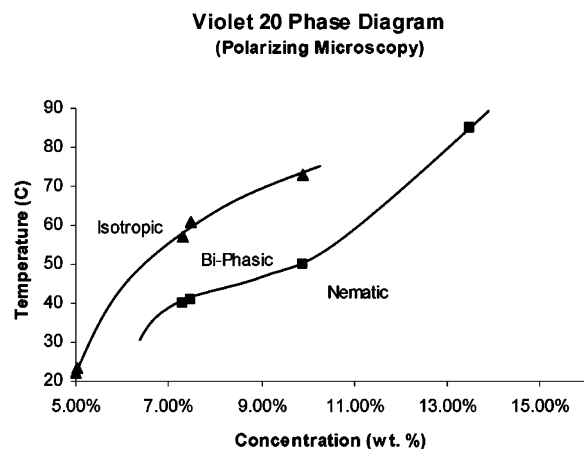


Figure 2. Phase diagram of aqueous solutions of Violet 20 as established by polarizing microscopy observations for thin (~ 20 μm) samples confined between two clean untreated glass plates.

along one direction, called the director \mathbf{n} . In this study, we used an 8% (wt) aqueous solution ($\text{pH} \approx 4$) of V20 that is in the uniaxial chromenematic N-phase at room temperature; see Figure 2.

We used PC Spartan Pro (Wavefunction, Inc.) to model the equilibrium geometry of isolated dye molecules and their pairs. The approximate "in-plane" dimensions of an isomer of Violet 20 are $7 \text{ \AA} \times 23 \text{ \AA}$ (Figure 1A). The typical molecule-to-molecule spacing along the LCLC columns that corresponds to the minimum of the interaction energy is about 3.4 \AA .¹⁶

Previously, we have demonstrated the macroscopic anisotropy of in-plane oriented monolayers and stacks of two, three, and four molecular layers of Violet 20 using an optical technique of absorption of linearly polarized light.⁶ In this work, we examine monolayers of molecular thickness with long-range in-plane orientational order by the supplementary techniques of atomic force microscopy (AFM) and X-ray photoelectron spectroscopy (XPS) which has a sampling depth of nanometers.

For imaging the LCLC by AFM, we examined mica, silica, and glass substrates. From the point of view of the substrate smoothness, mica is the best candidate, but there is a problem. The dye solution does not wet mica substrates well as the natural negative surface charge of the mica repels the negatively charged molecular cores of dye. To overcome this, we used two modified versions of the mica substrates of opposite (positive) polarity to the dye: commercially available AP mica (Bioforce Laboratory, Inc.) and ordinary mica coated in our laboratory with a polyion, poly(diallyldimethylammonium chloride) (PDDA, Aldrich, Figure 1B). For simplicity, the XPS surface analysis was done only on ordinary mica coated with polyion and dye.

XPS is a surface-specific technique with a sampling depth of less than 10 nm. It has the advantage of being nondestructive and providing both elemental and chemical information. Angle-resolved XPS (ARXPS) is capable of giving depth profile information without removing the top surface layers.¹⁷ ARXPS has been widely used to study Langmuir-Blodgett (LB) films¹⁸ and self-assembled monolayers (SAMs).^{19,20} In these systems, the organic film is usually attached to an inorganic substrate, and the depth information is derived from correlating the signal from the organic upper layer and signals from the inorganic substrate. However, not much work has been done using ARXPS to probe multilayer organic systems. Recently, it has been successfully applied to all-organic systems with multiple layers in studies of the photoalignment of thermotropic (solvent-

(16) Lydon, J. E. *Mol. Cryst. Liq. Cryst. Lett.* **1980**, *64*, 19–24.

(17) Cumpson, P. J. Angle-Resolved X-ray Photoelectron Spectroscopy. In *Surface Analysis by Auger and X-ray Photoelectron Spectroscopy*; Briggs, D., Grant, J. T., Eds.; IM Publications and Surface Spectra Limited: Chichester, Manchester, 2003.

(18) Solleti, J. M.; Botreau, M.; Sommer, F.; Brunat, W. L.; Kasas, S.; Duc, T. M.; Celio, M. R. *Langmuir* **1996**, *12*, 5379.

(19) Atanasoska, L.; Cammarata, V.; Stallman, B.; Kwan, W. S. V.; Miller, L. L. *Surf. Interface Anal.* **1992**, *18*, 163.

(20) Yamamoto, H.; Butera, R. A.; Gu, Y.; Waldeck, D. H. *Langmuir* **1999**, *15*, 8640.

independent) liquid crystals.²¹ A multilayered sample consisting of a Violet 20 monolayer on a PDDA layer on an inorganic substrate is an interesting complex organic system for ARXPS analysis. Using high-resolution spectra acquired from each individual component as templates, the C 1s and N 1s spectra of the multilayered system were curve-fitted and the orientation of the molecules was discerned.

All spectra were acquired on the Kratos AXIS Ultra photoelectron spectrometer. A monochromatic Al K α source was operated at 300 W. The base pressure was 2×10^{-10} Torr and the operating pressure was 2×10^{-9} Torr. Charge compensation was accomplished using low-energy electrons. Standard operating conditions for good charge compensation are -2.8 V bias voltage, -1.0 V filament voltage, and filament current of 2.1 A.

For X-ray photoelectron spectroscopic (XPS) analysis, a sample is placed in an ultrahigh vacuum environment, which is typically less than 10^{-8} Torr. The sample is then exposed to a low-energy, monochromatic X-ray beam, which causes the emission of photoelectrons from atomic shells of the molecules present on the surface. The simple theoretical relationship that describes this process is

$$E_k = h\nu - E_b - \phi_w \quad (1)$$

In this equation the kinetic energy E_k of the emitted photoelectron is the measured quantity, $h\nu$ is the known energy of the primary photon, and ϕ_w is the work function which accounts for the additional energy required to remove an electron from the sample surface to the vacuum. ϕ_w is a constant for the spectrometer. E_b , the binding energy for the emitted photoelectron, is the energy required to remove the electron from an atom. The emitted electrons possess an energy characteristic of the element and atomic orbital from which they are emitted. Formation of a chemical bond with another atom will change the energy of the ground state of the atom, which in turn will change the observed binding energy. This change in E_b is called a chemical shift. Hence XPS can provide chemical-bonding information.

Photoelectrons from the surface are directed into an electron energy analyzer, where they are separated according to energy and detected as a function of their kinetic energy, E_k . By counting the number of electrons detected at each energy value ($E_k < h\nu$), a spectrum of peaks corresponding to the elements on the surface is generated. The area under these peaks can be used to determine relative elemental compositions, while the shape and position of the peaks reflect the chemical environment of each element.

The kinetic energies of the photoelectrons leaving the sample are so low that, in practice, only those from the top 1–10 nm (the uppermost two through ten atomic layers) of the surface escape and arrive at the spectrometer without energy loss. Electrons originating from further below the surface will be reabsorbed or escape the surface with considerable energy loss. The information available from XPS is, therefore, highly specific to the surface of the material.

In ARXPS, changing the angle of the sample with respect to the direction probed by the detector, the so-called takeoff angle (TOA), one can vary the effective sampling depth.¹⁷ The approximate depth sampled, d , is given by the equation

$$d = 3\lambda \sin \theta \quad (2)$$

where λ is the inelastic mean free path of the photoelectron and θ is the angle between the sample surface and the detector acceptance direction.

Thus at $\theta = 90^\circ$ the sample surface is perpendicular to the line of acceptance of the analyzer, and d is the maximum sampling depth of 3λ . As θ is reduced, the sampling depth decreases as seen in Figure 3.

Large area surveys were acquired for 3 min using a pass energy of 80 eV. High-resolution spectra were acquired using a pass energy of 20 eV. Takeoff angles of 90, 60, and 30° were utilized in the acquisition of high energy resolution spectra. The C 1s spectra were acquired over the E_b range of 290–279 eV for 8 min, the N 1s spectra were acquired for 15 min from 403 to 393 eV,

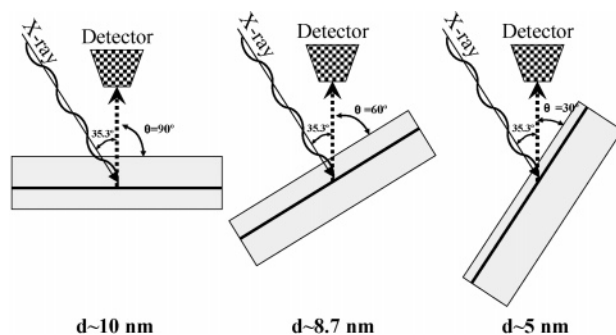


Figure 3. The principle of angle-resolved XPS analysis. By tilting the sample with respect to the detector, the sampling depth decreases from approximately 10 nm for 90° to approximately 5 nm at 30°.

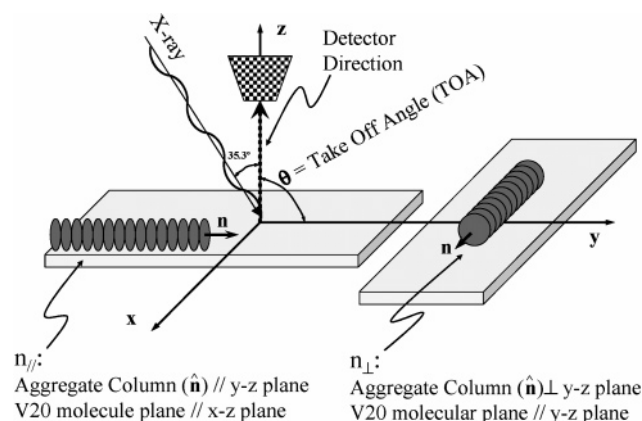


Figure 4. The scheme of XPS analysis. The average orientation of the aggregate columns (director \mathbf{n}) is either in the plane of the incident X-ray beam (left, state n_{\parallel}) or perpendicular to this plane (right, state n_{\perp}) and detector direction angle is fixed at 35.3°, and the sample is rotated azimuthally in the x – y plane for n_{\perp} and n_{\parallel} cases.

and the S 2p spectra were acquired from 170 to 162 eV for 15 min. All O 1s spectra were acquired for 5 min in a range of 533–524 eV.

Initially, the spectra were analyzed as a function of the orientation of the LCLC director in the plane of the deposited film for a fixed TOA, to study the structural anisotropy of the monomolecular film. We examined two orientations of the director \mathbf{n} that specifies the average orientation of the aggregates in the plane of the film, with respect to the X-ray plane of incidence. In the first geometry, labeled n_{\parallel} , the director is parallel to the plane of the X-ray incidence (left part of Figure 4); in the second geometry, labeled n_{\perp} , the director is perpendicular to the plane of X-ray incidence. These two geometries were first studied at one fixed value of the TOA, say 90°, and then the TOA was changed, the two geometries n_{\parallel} and n_{\perp} were analyzed again, etc. We performed the studies for a variety of samples, including PDDA monolayers and thick PDDA coatings on mica (with no LCLC aggregates) and multilayered composites with a layer of LCLC material (V20) over the PDDA and mica. Four areas per sample were analyzed. Data analysis and quantification were performed using the Vision software provided by the manufacturer. A linear background was used for quantification and curve fitting of the high-resolution spectra. Quantification utilized sensitivity factors provided by the manufacturer. Curve fitting was carried out using the spectra of individual components as templates as explained in the next section.

Results

A. AFM. AP mica is freshly cleaved mica that has been treated with aminopropyltriethoxysilane ($\text{H}_2\text{N}(\text{CH}_2)_3\text{Si}(\text{OC}_2\text{H}_5)_3$) to reverse the sign of the electric charge at its surface. This process produces a surface with positively charged amino groups.²² We prepared the dye samples on

(21) Su, L.; West, J. L.; Artyushkova, K.; Fulghum, J. E.; Reznikov, Yu. *J. Electron Spectrosc. Relat. Phenom.*, in preparation.

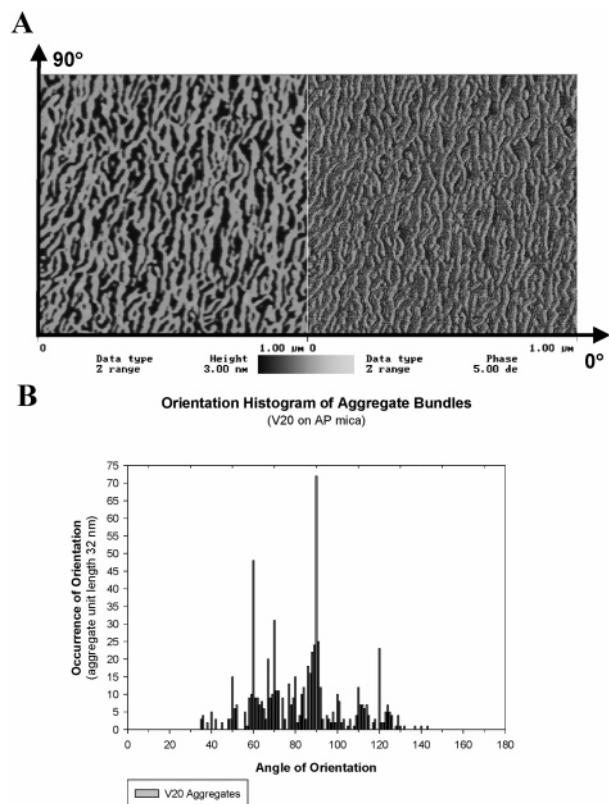


Figure 5. (A) AFM image of V20 on AP mica. (B) Orientational histogram denoting the average orientation of the elongation of the V20 aggregate bundles. The orientation was measured by dividing the AFM image into 32×32 nm pixels and determining the average orientation of the aggregate bundle within the pixel. Note shear deposition direction corresponds to approximately 90° in the AFM image.

AP mica by shearing an 8% solution of V20 dye in water onto the substrate and then letting the sample sit in a humid environment for 5 min. We rinsed the substrates with deionized water to remove all but the thin layer of dye that adhered to the positively charged substrate. The samples were then quickly dried by a nitrogen stream. In Figure 5A, we see the height data on the left (increasing brightness means increasing height) and the phase contrast on the right (increasing brightness means increasing friction). This image indicates the AP treatment was, most likely, too highly charged to be effective for imaging dye aggregates, as there was no flat surface on the mica for reference, and the thickness of the dye layer was unknown. However, in Figure 5B, we can see an average orientation of the elongated aggregate bundles of about 90° ; i.e., the aggregates align along the shear deposition direction. It is interesting to note that in Figure 5B there appear to be two other weaker orientations at $\pm 30^\circ$ with respect to the shearing direction. These additional directions might be caused by such factors as (a) the anisotropic anchoring interaction of the LCLC aggregates with the crystalline lattice of mica, (b) a tilted association of V20 molecules within the aggregates that occurs after transfer from the solution to the substrate, or (c) the viscoelastic behavior of the LCLC during the shear deposition. To find out the prevailing factor(s), more experiments are needed as well as a full-scale statistical analysis of the orientational pattern left by the LCLC monolayer on different substrates. Such a study is planned for the future.

To create mica substrates with polyion coatings, we applied a double-stick tape to both sides of the mica and

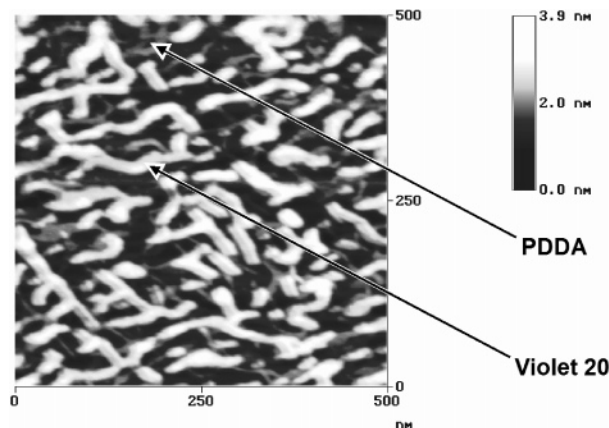


Figure 6. AFM image of mica substrate. V20 appears thick (20–40 nm wide) and bright (1–2 nm high), whereas PDDA appears dim (<1 nm high).

peeled it off to produce a fresh negatively charged surface on either side. Excess mica flakes were blown off with a nitrogen stream. To reverse the surface charge, the mica substrates were then immersed for 20 min in a dilute solution of 2 mg/mL PDDA (Figure 1B) in water. This positively charged polyion adhered to the negatively charged surface. We then rinsed the substrates in ultra-pure deionized water to remove the excess PDDA. N-phase solutions of V20 were sheared over the mica substrate with a clean rubber finger clot. After 5 min, the excess dye was rinsed off with deionized water. The amount of time the dye is allowed to adsorb on the surface, in general, determines the surface coverage of the material. To achieve a good signal-to-noise ratio in imaging aggregate columns, i.e., to distinguish them from the background, 5 min of adsorption time was found to be sufficient. In Figure 6, the 500 nm scan reveals dye aggregate bundles that are 20–40 nm in width, 1–2 nm in height, and from 40 nm to more than 300 nm long. Interestingly, recent light scattering experiments performed for aqueous solutions of disodium cromoglycate (DSCG) LCLC at temperatures slightly above the nematic-to-isotropic phase transitions reveal that the length of molecular aggregates is about 10–20 nm,²³ consistent with the observation of the somewhat longer aggregates in the films deposited from the V20 nematic phase.

A large-scale scan of V20 in Figure 7A shows that the shearing direction can control the orientation of dye aggregates. In this scan, one extra layer was cleaved from the substrate revealing a “nanocanyon” with 1 nm walls where the floor is lower than its surroundings (the darker diagonal middle strip in Figure 7A). Because the surface here is lower, the dye fell into this “nanocanyon” and the influence of the shearing force was probably somewhat lessened. The dye aggregate bundles (streaks) on the lower surface are oriented differently from the dye streaks on the top surface. This implies that the shearing did, in fact, orient the dye on the higher surfaces as is evident in Figure 7B. The aggregates in the “nanocanyon” tend to align parallel to the canyon walls, as indicated by the largest orientational peak in Figure 7C. This suggests a possible confinement-induced alignment, which is natural, as the width of the “nanocanyon” is only about 300 nm, i.e., on the same order as the length of the aggregates.

(22) Bezanilla, M.; Manne, S.; Laney, D. E.; Lyubchenko, Y. L.; Hansma, H. G. *Langmuir* **1995**, *11*, 655–659.

(23) Nastishin, Yu. A.; Liu, H.; Shiyankovskii, S. V.; Lavrentovich, O. D.; Kostko, A. F.; Anisimov, M. A. *Phys. Rev. E* **2004**, *70*, 051706.

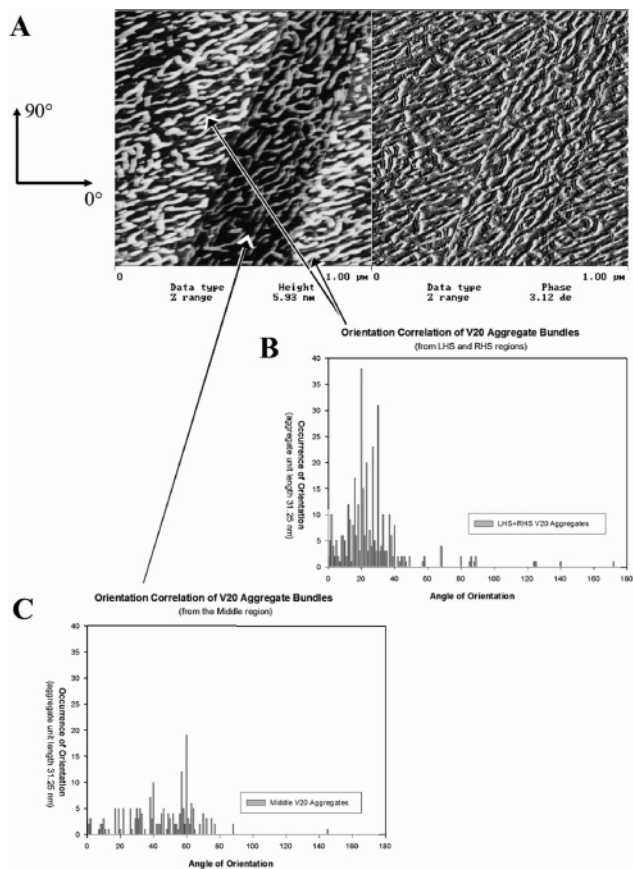


Figure 7. (A) AFM image of a “nanocanyon” in the mica. This reveals the true shear orientation direction of the V20 aggregate bundles. (B, C) Orientational histograms denoting the average orientation of the elongation of the V20 aggregate bundles in the high (B) and low (C) areas of the AFM image. Note the walls of the “nanocanyon” are oriented at a 60° angle which corresponds to the largest orientational peak in (C).

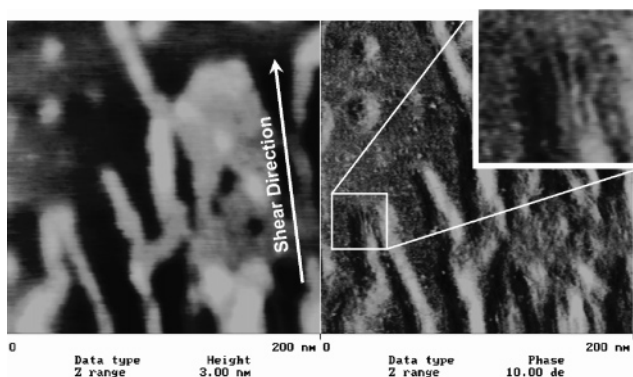


Figure 8. AFM image of V20 aggregate columns forming aggregate bundles. Note the columns are generally 1–2 nm in width and 1–2 nm apart. They appear as fingers extending from the aggregate bundle.

By carefully adjusting the AFM settings, we were able to resolve the aggregate columns of V20, which compose the aggregate bundle streaks in Figure 8. Note that the aggregate columns visible in the inset with an enlarged view in Figure 8 are elongated in the same direction as the streaks, which implies that the axes of columns are elongated in the shearing direction. Due to the high signal-to-noise ratio of these samples, we were able to take 20 nm scans of the dyes in tapping mode in Figure 9. Although the height data were poor, the phase data shown in Figure 9 revealed what seemed to be actual aggregates of the dye

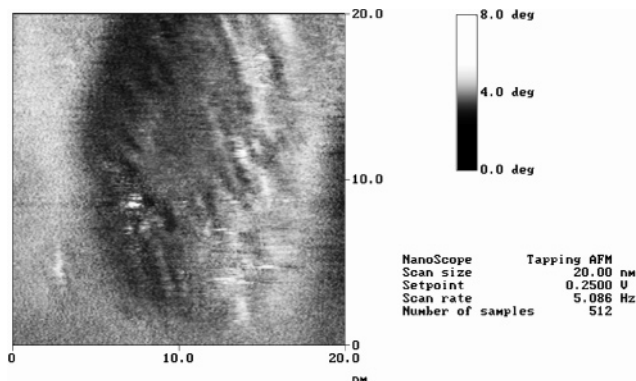


Figure 9. High-resolution (20 nm) AFM image of V20 aggregate columns forming an aggregate bundle. Note the individual columnar mesogens of the V20 aggregates are parallel to each other and are 1–2 nm wide and 1–2 nm apart.

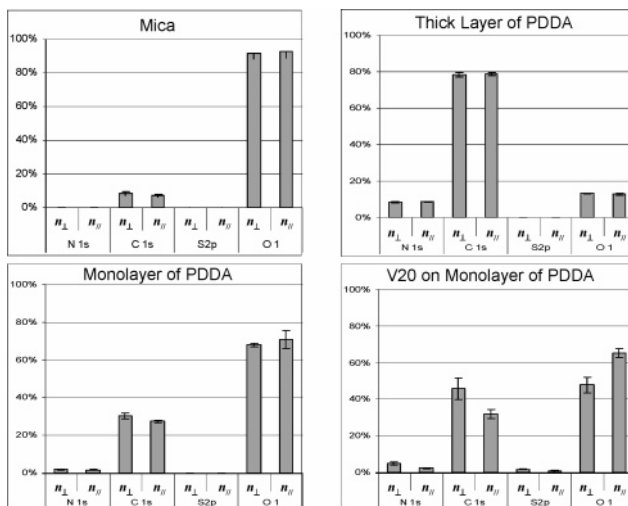


Figure 10. Elemental composition for thick PDDA, monolayer PDDA, and V20 on monolayer PDDA samples. Results are shown for both $n_{||}$ and n_{\perp} geometries, side by side, for comparison.

elongated in the shearing direction. These appeared as slender cylinder-like features on a clump of dye (aggregate bundle) where the cylinders were 1–2 nm wide, 1–2 nm tall, and 1–2 nm apart.

B. XPS. A cleaned mica sample, samples of a PDDA monolayer, and thick PDDA on mica were analyzed by XPS at the same time as the multilayered samples. On clean mica, no nitrogen and 6% C were detected. This carbon contamination consists of hydrocarbons and oxygen-containing species. Figure 10 shows elemental compositions for mica, thick ($\sim 1 \mu\text{m}$) PDDA, a PDDA monolayer, and V20 on a PDDA monolayer for $n_{||}$ and n_{\perp} geometries (Figure 4). Results shown are the average of four analyses per sample. For both the thick PDDA and PDDA monolayer samples on mica, the elemental compositions for the $n_{||}$ and n_{\perp} geometries are very similar. Note here that, in the case of PDDA or pure mica samples, there are no LCLC aggregates at the substrates; thus the notations $n_{||}$ and n_{\perp} are used for the sake of comparison with the LCLC films in which the director might be either in the plane of the X-ray incidence, $n_{||}$, or perpendicular to it, n_{\perp} , Figure 4. The thick PDDA sample contains 8% N, while the monolayer sample contains 2% N. The strong oxygen signal from the PDDA monolayer sample is a result of oxygen in the mica substrate, as the layer is thinner than the XPS sampling depth.

For the V20 monolayer sample, elemental quantification results for sample orientations $n_{||}$ and n_{\perp} are quite different.

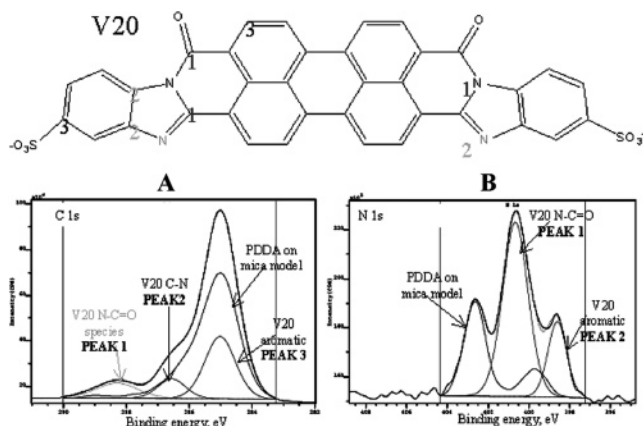


Figure 11. V20 formula (top). Curve fit of high-resolution (A) C 1s and (B) N 1s spectra from V20 on PDDA using a model photopeak of PDDA monolayer on mica and peaks due to V20. Chemical species and corresponding peaks in curve fit are marked with numbers.

Even taking into account standard deviations for sampling, this significant difference suggests some orientational order of V20 in the plane of the film. The 1–2% S and 2–5% N that are detected for the multilayered sample are from the layer of V20. The significant signal due to oxygen for this sample is a combination of oxygen present in the mica and the V20 monolayer.

Figure 11 shows the formula of V20, in which all of the chemical species of carbon and nitrogen that are distinguishable in XPS spectra are labeled. Five types of carbons are present in V20, including N–C=O, N–C=N, aromatic C, aromatic C–N, and C–SO₃⁻ species. These five carbon species will be distinguished in three separate peaks in the C 1s high-resolution spectra. N–C=O and N–C=N species will have approximately the same shift of 3–3.5 eV (peak 1). C–SO₃⁻ will have a small shift of -0.2 eV, similar to the position of the aromatic C (peak 3). Very small amounts of S were detected, so no separate peak for C–SO₃⁻ was utilized. The third peak at 286.5 eV (peak 2) is due to C–N species.

Figure 11 shows the approach to curve fitting the C 1s and N 1s spectra from the multilayered sample. The model C 1s photopeak from the PDDA monolayer on mica is applied first (Figure 11A). This model photopeak contains contributions from the carbon present in both the PDDA monolayer and the hydrocarbon contamination on mica. The position of this peak is constrained to that observed in the PDDA monolayer on mica sample. The height of this peak is constrained by its width. The aromatic carbons in V20 result in a narrower peak at low E_b than the mix of aliphatic and aromatic carbons contained in PDDA. If the PDDA component is increased in intensity, it is too broad to fit the low binding energy component. Finally, three peaks due to V20 are added at the positions of binding energies identified by the previous discussion.

Figure 11B shows the N 1s curve fit of V20 on PDDA. The shape of the N 1s peak is unique, and there is less ambiguity in curve fitting of this spectrum than in C 1s. Two types of N are present in V20 as shown in Figure 11: aromatic N and N–C=O species. Two peaks for these types of N are used to curve fit the N 1s spectrum of the multilayered sample together with the N 1s model shape of the PDDA on mica sample. In this case, the PDDA component is constrained by the height of the peak at 402.7 eV.

High-resolution C 1s and N 1s spectra were fitted in this manner for all TOAs and for $n_{||}$ and n_{\perp} data. Figure

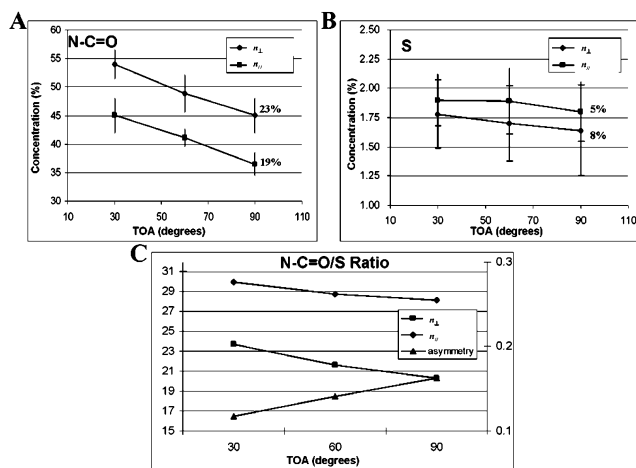


Figure 12. (A) Raw data illustrating the drop in N–C=O with increasing TOA. (B) Raw data illustrating that S remains relatively constant with increasing TOA. (C) Ratio data combining (A) and (B) clearly demonstrating anisotropy in the film for the $n_{||}$ and n_{\perp} cases. The asymmetry between sample orientations $n_{||}$ and n_{\perp} increases with increase of TOA.

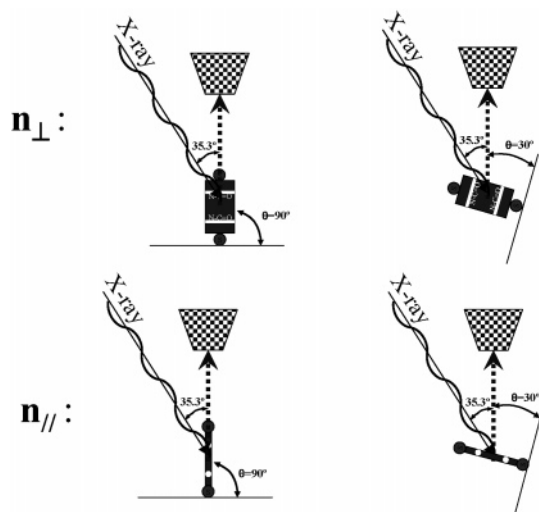


Figure 13. Signals from N–C=O. At left, we can see that for large TOA (deeper sampling depth) the signal from N–C=O is screened, whereas at right we can see that the signal from N–C=O is enhanced for small TOA (shallower sampling depth).

12A shows that the amount of N–C=O species decreases with increasing TOA. There is a difference in the percentage of N–C=O species observed for the $n_{||}$ (45%) versus n_{\perp} (37%) case. However, the relative increase of those species with decreasing depth is approximately the same at 20%. Taking into account the small S concentrations and large standard deviations, as shown in Figure 12B, the decrease in S can be viewed as negligible compared to the error of the experiment, and we can consider the S signal constant throughout the sampling depth. Ratios of these two species (N–C=O/S) show changes in slope, and it is larger for the $n_{||}$ sample (16%) than for the n_{\perp} sample (10%). The reason for this decrease of N–C=O/S ratio with increasing TOA is mainly the decrease of N–C=O signal, as shown in Figure 13. The asymmetry function was calculated according to $A = (I^{n_{\perp}} - I^{n_{||}})/(I^{n_{\perp}} + I^{n_{||}})$, where I is the ratio of N–C=O/S for n_{\perp} and $n_{||}$ sample orientations. The asymmetry function is plotted in Figure 12C, demonstrating that the anisotropy is more pronounced for 90° TOA than for 30° TOA.

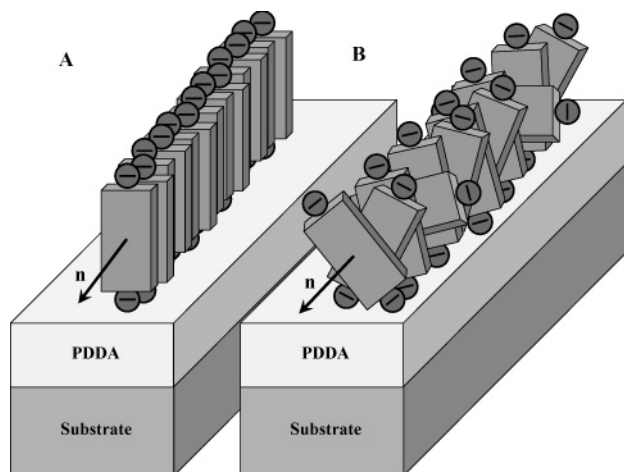


Figure 14. (A) An aggregate column where all the molecular planes are parallel. (B) An aggregate column where the molecular cores are randomly rotated about the columnar axis, yet remain parallel with respect to each other.

Discussion

From the AFM results, as we have discussed (see Figure 8, for example), we can conclude that the aggregates are preserved within the monolayer of a dried LCLC material. In addition, we can clearly see that the aggregates adsorb on the surface, maximizing the exposure of the charged groups of the columnar LCLC aggregates to the charge on the surface. That is, the columns align parallel to the substrate surface rather than standing perpendicular. However, it is not clear to what degree the surface adsorption preserves the intraaggregate features of molecular packing, i.e., the azimuthal orientation of molecules around the axes of the columnar aggregates. One can suggest two extreme types of intraaggregate geometries: one where all of the molecules have the same azimuthal angle (a biaxial aggregate) and one where the angle changes from molecule to molecule in a random fashion so that only the polyaromatic cores lie parallel to each other (giving an aggregate a uniaxial cylindrical symmetry); see parts A and B, respectively, of Figure 14. Of course, all intermediate geometries with different degrees of freedom for molecular rotation within the aggregate are possible. In addition, when the aggregates are transferred from the solution to the substrate, one might also expect that electrostatic interactions might alter the tilt of the molecular planes with respect to the axes of the aggregates. Examinations of (wet) N-phase solutions of V20 in cells in which the director aligns perpendicular to the bounding plates (homeotropic anchoring) indicate that the bulk of the N-phase is optically uniaxial—no second “director” axis is observed, which implies that either the aggregates themselves or their packing is of a cylindrical symmetry with the axis along the axis of the aggregates. Such a uniaxial symmetry would be broken at the substrate, but it is hard to expect the completely ordered structure depicted in Figure 14A because of the electrostatic repulsions between the extremities of the V20 molecules that are not in contact with the substrate. Additionally, if we take into consideration that V20 is a mixture of isomers (Figure 1), we can see that there may be some inherent offset spacing between the like-charged groups (Figure 14B) or lateral shift of the molecules along the substrate. Recent spectroscopic studies of an LCLC system structurally similar to V20 have indicated the possible existence of rotated dimers within the aggregate structure.²⁴

The application of ARXPS to probe anisotropic dried LCLC films reveals the sensitivity of the XPS signal to the orientation of the organic molecules at the substrate. The data in Figure 12 demonstrate that the spectra are sensitive to the anisotropy of the in-plane-oriented LCLC monolayers on the mica substrate (or, at least, the particular chemical groups associated exclusively with V20). In principle, there might be three possible explanations for this: (1) an electron channeling effect, (2) a peripheral effect due to the aperture on the detector, or (3) polarization of the X-ray beam. It is unlikely that the observed effect of orientational sensitivity is due to electron channeling because it is most pronounced at 90° TOA and less pronounced at shallower TOAs. If electrons were channeling within the V20 monolayer, it would be expected that the opposite would be true; i.e., the anisotropy would be more pronounced at the shallower TOA as the shallower sampling depth guarantees a longer path through V20 for photoelectron escape. Regarding the peripheral effect due to the aperture of the slit opening on the detector, the analyzer samples an area of approximately 300 μm × 700 μm. It is obvious from Figures 5–7 that the features of interest are much smaller than this analysis area size and therefore homogeneous coverage should be detected in either case of sample orientation, with the director being in the plane of X-ray incidence, $n_{||}$, or perpendicular to it, n_{\perp} . Therefore, the most reasonable explanation of the observed orientation dependence of the XPS signal is partial polarization of the probing X-ray beam²⁵ coupled with the structural in-plane anisotropy of the films prepared from LCLCs. Such partial polarization is entirely possible as the X-rays are monochromatized by the process of diffraction off arranged quartz crystals placed on a toroidal backplane of a Rowland circle. The polarized beam may, thus, cause dichroism in photoelectron emission from particular bonds of oriented LCLC molecules, aligned in different ways with respect to the X-ray polarization, providing, as a result, differentiation between those bonds. This sensitivity of large area XPS analyses to orientational chemical structure of materials was observed for other model systems with known orientation and aligning properties.²⁶ Note that no difference between the two sample orientations depicted in Figure 4 was observed for structures with no LCLC aggregates, such as clean mica, thin and thick PDDA layers on mica; see Figure 10.

Circular dichroism in the angular distribution (CDAD) and linear dichroism in angular distribution (LDAD) are well-known phenomena utilized for molecular orientation studies in synchrotron radiation sources with high circular or linear polarization of the out-of-plane radiation. CDAD of photoelectrons measures the difference in photoelectron intensities for circular polarized light emitted at a definite angle. It necessarily requires alignment or orientation of the initial state. Circular dichroic effects in photoemission and photoadsorption were first observed for magnetic materials, where the combined action of exchange and spin–orbit interactions leads to helicity-dependent photoadsorption and photoemission intensities.^{27,28} Circular

(24) Camorani, P.; Furier, M.; Kachkovskii, O.; Piryatinskiy, Yu.; Slominskii, Yu.; Nazarenko, V. *Semicond. Phys., Quantum Electron. Optoelectron.* **2001**, *4*, 229.

(25) Surman, D. Kratos. Private communication, Feb 6, 2004.

(26) Pylypenko, S.; Artyushkova, K.; Fulghum, J. E.; Su, L.; West, J. L.; Reznikov, Y. Ion Beam Alignment of Liquid Crystals on Polymer Substrates. Presented at the AVS 50th International Symposium, 2003, Baltimore, MD.

(27) Bansmann, J.; Lu, L.; Meiwes-Broer, K. H.; Schlatholter, T.; Braun, J. *Phys. Rev. B* **1999**, *60*, 13860.

(28) van der Laan, G. *J. Magn. Magn. Mater.* **1995**, *148*, 53.

dichroic effects have been theoretically predicted²⁹ and experimentally verified in photoemission from aligned^{30,31} and spatially fixed molecules³² and nonferromagnetic solids.³³ For XPS analysis of aligned molecules using conventional X-ray sources, partial polarization of incoming X-ray sources may cause a smaller, but detectable, dichroism in emission at various TOAs.

Conclusion

Oriented monolayers of the lyotropic chromonic liquid crystal Violet 20 were imaged on mica and PDPA substrates. Individual aggregate columns of LCLC material were visualized using atomic force microscopy and

(29) Dubs, R. L.; Dixit, S. N.; McKoy, V. *Phys. Rev. Lett.* **1985**, *54*, 1249.

(30) Appling, J. R.; White, M. G.; Kessier, W. J.; Fernandez, R.; Poliakoff, E. D. *J. Chem. Phys.* **1988**, *88*, 2300.

(31) Appling, J. R.; White, M. G.; Dixit, S. N.; McKoy, V. *J. Chem. Phys.* **1987**, *87*, 6927.

(32) Westphal, C.; Bansmann, J.; Getzlaff, M.; Schonsense, G. *Phys. Rev. Lett.* **1989**, *62*, 151.

(33) Schonhense, G. *Phys. Scr., T* **1990**, *31*, 255.

verified to be of the same approximate dimensions as the individual molecule, 1–2 nm in height and width. The columns were found to be highly oriented. XPS was employed to probe the films and verify the elemental composition. XPS was found to be sensitive to the orientational anisotropy of the in-plane-aligned monolayers of LCLC.

Acknowledgment. We thank Sergij Shiyonovskii for fruitful discussions. This material is based upon work supported by NSF/ITIC 03-569 (DMR-0346348), NSF CHE-9613880, and UNM. The XPS was funded by a grant from the Keck Foundation, NSF CHE-0113724, and UNM. We gratefully acknowledge the generous donation by Mrs. Glenn H. (Jessie) Brown in support of this research, partial support by the Ohio Board of Regents, and the NSF Science and Technology Center for Advanced Liquid Crystalline Optical Materials (ALCOM) under Contract No. DMR 89-20147.

LA047788+